Proceedings of the 49th International School and Conference on the Physics of Semiconductors "Jaszowiec 2021"

Properties of Thin MgO Films on 6H–SiC and GaN: Photoelectron Studies

R. Lewandków*, M. Grodzicki, P. Mazur and A. Ciszewski

Institute of Experimental Physics, University of Wrocław, pl. M. Borna 9, Wrocław, Poland

Doi: 10.12693/APhysPolA.141.116 *e-mail: rafal.lewandkow@uwr.edu.pl

Properties of MgO layers on p-GaN(0001) and p-6H–SiC(0001) surfaces are studied using X-ray and ultraviolet photoelectron spectroscopy. Up to 5 nm thickness, MgO thin films have been deposited *in situ* under ultrahigh vacuum by electron beam evaporation. The formation of MgO compound with Mg 2*p* and O 1*s* core levels located at 51.0 eV and 531.6 eV, respectively, is confirmed by X-ray photoelectron spectroscopy. The bandgap widths of MgO films determined from the Mg 2*p* and O 1*s* losses are estimated to be 6.7 eV and 6.9 eV for MgO layers with a thickness of 5 nm deposited on SiC and GaN substrates, respectively. Valence band maxima of bare substrates and MgO films are found from the ultraviolet spectra. Offsets of the valence and conduction bands have been calculated. Their respective values are 1.9 eV and 1.8 eV for the MgO/SiC interface, and 2.3 eV and 1.2 eV for the MgO/GaN interface.

topics: p-GaN, 6H–SiC, MgO/6H–SiC, MgO/p-GaN interface, valence band, photoelectron spectroscopy

1. Introduction

Wide bandgap semiconductors for high-power/high-frequency devices have been widely studied over the years. Silicon carbide (SiC) and gallium nitride (GaN) are well-established materials for such applications [1–3]. Both owe their high market position to good physical properties, such as high thermal conductivity, wide bandgap, high maximum current density, and high breakdown voltage [4–7]. Both have high chemical and thermal resistivity due to their hardness, which allows electronic devices to work under demanding conditions [3].

Dielectric/semiconductor interfaces are integrated parts of a semiconductor device. On the one hand, they are an active part of the electronic device and, on the other hand, they can be the result of the formation of isolation or covering in integrated circuits. There are many factors that can have an impact on the performance of SiC and GaN-based devices, such as the surface preparation method or the thin film deposition method. Since the application of a dielectric layer can improve the performance of the power devices [8], high dielectric constant and wide bandgap materials are desired for SiC and GaN-based devices. Dielectric/p-type and n-type semiconductor interfaces are of particular interest, as both types of regions function as critical device components [9, 10]. Many oxides have been tested over the years for this application and several suitable candidates have emerged, such as tantalum oxide (Ta_2O_5), aluminum oxide (Al_2O_3), nickel oxide (NiO), hafnium oxide (HfO_2), and magnesium oxide (MgO) [8, 11–14]. GaN and SiC hexagonal crystal structure present a challenge to oxide growth, for example, twinning and faceting resulting from symmetry and surface energies [15]. Among the considered oxides, MgO seems to be one of the best candidates for a buffer layer. It has a large dielectric constant and a wide bandgap. Moreover, it is a cubic oxide that has a relatively low lattice mismatch with SiC and GaN. Among the methods used so far for thin MgO layers deposition on GaN as well as on SiC, molecular beam epitaxy (MBE) seems to be most used [16–19], however different methods such as atomic layer deposition (ALD) [20], sol–gel route [21], and electron beam evaporation [22] were also applied.

One of the most important characteristics of the interface are the valence and conduction band offsets (VBO and CBO) [13, 23, 24], which can be affected by the quality of the deposited oxide layer and the deposition method. Magnesium oxide is a widely studied high-k oxide on SiC and GaN, however most of the research focuses on the deposition methods [16, 18, 21, 25] or bandgap measurements [25, 26]. Much less research focused on band offsets for the systems has been conducted. There are only a few studies on MgO/GaN [23] and MgO/4H–SiC [27] related to this issue.

This report presents combined X-ray and ultraviolet photoelectron spectroscopy (XPS and UPS) investigation of MgO layers deposited by electron beam evaporation on both p-type semiconductors. The results show the physicochemical properties of MgO/GaN(0001) and MgO/6H–SiC(0001) heterojunctions, focusing on the band offsets at the interfaces. The aim of this report is to check if the studied MgO layers deposited by the electron beam evaporator on GaN and SiC will have sufficient band offsets to be considered as a barrier for the carriers.

2. Materials and methods

Samples of about 10×5 mm^2 are applied as substrates for these studies. In the case of 6H–SiC samples, they were cut from a wafer (CREE) with the Al-doped p-type homoepitaxial 6H–SiC layers (the concentration density of Al, $N_a = 7 \times 10^{15}$ cm^{-3}). The p-type GaN samples were cut from a Al_2O_3 wafer with Mg-doped GaN layer (5 μm thick) grown by metalorganic chemical vapor deposition (TDI Inc.) (the concentration density of Mg, $N_a = 5 \times 10^{16}$ cm^{-3}).

First, the substrates are cleaned *ex situ* by dousing in alcohol and rinsing with distilled water, then they are mounted on Mo plates and placed into the UHV chamber with a base pressure $\approx 1 \times 10^{-10}$ Torr. After that, the substrates are cleaned *in situ* by cycles of annealing at 800°C. Bare substrates and the MgO/6H–SiC, MgO/p-GaN interfaces are characterized in a SPECS surface analysis system using XPS with Mg K_α (1253.6 eV) and Al K_α (1486.6 eV) radiation sources, and by UPS with the He(I) (21.2 eV) line, from a DC discharged lamp with two-stage differential pumping (UVS 10/35). Additionally, low electron energy diffraction (LEED) is studied with an ErLEED 3000D camera. A hemispherical electron energy analyzer (HAS, Phoibos 100), with a take-off angle of 90°C, is used in a constant analyzer energy (CAE) mode. To measure core levels and valence bands, pass energies of 10 eV and 2 eV are used in steps of 0.1 eV and 0.025 eV, respectively. The MgO layers were deposited under ultrahigh vacuum (UHV) conditions at room temperature (RT).

The magnesium oxide films have been evaporated by electron beam evaporation using 99.95% pure MgO pieces (Kurt Lesker) as an evaporation source. After the film deposition, the sample is characterized at RT by the XPS and UPS, and the deposition process is repeated. Film thickness is estimated based on the XPS measurements from the relative intensity of the Ga 3*d* peak in the case of GaN and the C 1*s* peak in the case of SiC [28–31].

The Fermi level (E_F) position is determined from the Ar-cleaned Au reference sample to which all the spectra obtained are related. A Prisma 200 quadrupole mass spectrometer is used to monitor the residual gas composition in the chamber. The UV spectra are measured with -5 V and -10 V bias to obtain clean cut-off energy (E_{cutoff}) in addition to the measurement in the state of electrical equilibrium. XPS and UPS spectra are analyzed with CasaXPS software (ver. 2.3.19PR1.0) using Gaussian and Lorentzian GL(60) line shapes with Shirley background for peak fitting. All measurements are performed *in situ* under UHV at RT.

The procedure proposed by Greczynski and Hultman [32–34] has been used for checking sample charging. It is based on the assumption that the sum of the binding energy of the C–C bonding and the work function ϕ_S of the measured sample is constant, i.e., $E_B^{(\text{C}-\text{C})} + \phi_S = 289.58 \pm 0.14$ eV. The binding energy correction for the peaks has been applied for the samples where the relation differs by more than the error. After the whole cleaning procedure, the p-GaN exhibits a small amount of carbon and oxygen contamination ($\approx 4\%$). In the case of SiC samples, the oxygen contamination was almost completely removed, but the surface was enriched with carbon due to carburizing [32, 35].

3. Results and discussion

Main XPS signals from the MgO/6H–SiC thin films are shown in Fig. 1. The Si 2*p* and C 1*s* core level lines of the p-6H–SiC substrate decline following the MgO film growth (see Fig. 1a and b). Binding energy (BE) and full width at half-maximum (FWHM) of the Si 2*p* peak amount to 101.7 eV and 1.4 eV, respectively. After a deposition of a 5 nm thick MgO film, the Si 2*p* peak shifts slightly 0.1 eV towards higher BE values. The shift does not exceed the value of an error limit of the energy evaluation. The C 1*s* core level spectrum can be fitted with two components, similar to the fittings reported earlier [36–39]. With the BE value of 283.8 eV and the FWHM value equal to 1.1 eV, the main line is attributed to Si–C bonds consistently with the other studies [40–43]. The smaller BE component equal to 285.4 eV can be attributed to carbonaceous contaminants [41]. As opposed to the prior report [44], the LEED patterns observed here exhibit (1×1) structure with no additional spots, which excludes graphene termination as described in our previous work [38]. The position of the C 1*s* peak remains the same throughout the experiment.

For a bare p-6H–SiC(0001) surface, the Mg 2*p* signal is not observed (see Fig. 1c) and the O 1*s* signal is barely visible (see Fig. 1d). The deposition of the MgO film results in the formation of the O 1*s* and Mg 2*p* peaks, for which the BE values, in the case of a 3 nm thick film, are respectively 531.6 eV and 51.2 eV. The FWHM of the latter is 1.4 eV, and the new peak position is shifted by about 1 eV towards higher BE values with respect to the position of the Mg 2*p* line reported for metallic Mg [45]. Such a location of the peak indicates that the XPS signal arises from the MgO compound [46, 47], which was confirmed independently by means of two XPS databases [45, 48].

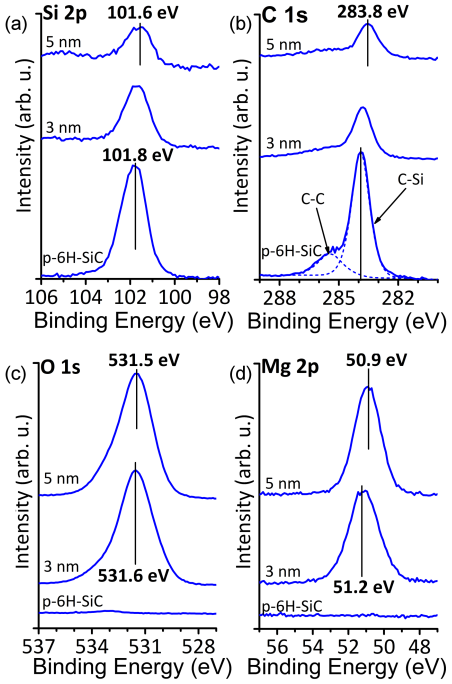

Fig. 1. The XPS spectra of (a) Si 2*p*, (b) C 1*s*, (c) O 1*s*, and (d) Mg 2*p* core lines of the p-6H–SiC(0001) surface before and after deposition of the MgO films of the average thickness of 3 and 5 nm.

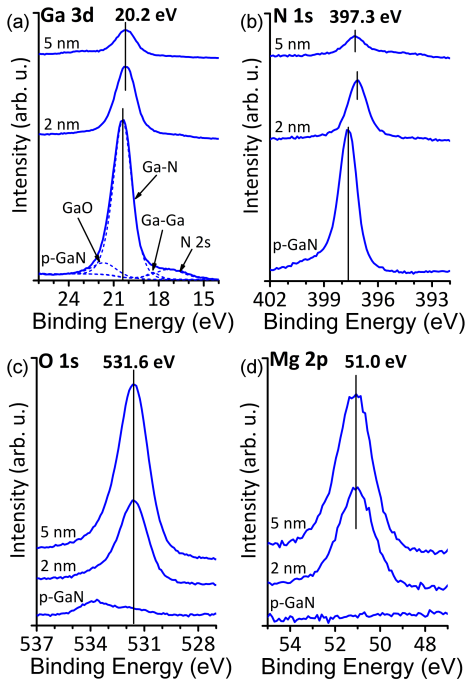

Fig. 2. The XPS spectra of (a) Ga 3*d*, (b) N 1*s*, (c) O 1*s*, (d) Mg 2*p* core lines of the bare p-GaN (0001) surface and covered with MgO films.

The major features of the XPS spectra collected for the MgO/p-GaN system are presented in Fig. 2. For the bare substrate, the Ga 3*d* BE amounts to 20.4 eV with 1.5 eV FWHM (see Fig. 1a). Cycles of annealing at 800°C under UHV may remove surface impurities, as well as decompose chemical stoichiometry of the surface. So to preserve acceptable surface stoichiometry, the annealing treatment must be interrupted when some remainders of oxygen impurities are still present on the surface (see bare p-GaN spectrum in Fig. 2c). This leads to the depletion of the subsurface layers of p-type carriers and, consequently, to the presence of an inversion layer, as has been reported in [49]. Complementary LEED investigation of the bare p-GaN (0001) substrate after the annealing, exhibits the (1×1) structure despite the presence of some of the oxide reminders mentioned above. The Ga 3*d* signal can be deconvoluted into four components coming from Ga–O, Ga–N, Ga–Ga bonds and overlapping of the N 2*s* state [50] (see Fig. 2a). After the MgO deposition, the Ga 3*d* line shifts slightly towards the lower BEs, finally locating at 20.2 eV. Similar behaviour is observed for the N 1*s* core level line. For the bare substrate, the N 1*s* line has BE of 397.6 eV with 1.1 eV FWHM and it shifts after the MgO layers deposition, reaching a value of 397.3 eV (see Fig. 2b). The O 1*s* core level line resulting from MgO located at 531.6 eV is independent of the MgO film thickness (see Fig. 2c), likewise, the Mg 2*p* line is positioned at 51.0 eV (see Fig. 2d).

The UPS spectra of the valence band (VB) for both substrates are typical for semiconductors (see Fig. 3b and d). The valence bands are located below the Fermi level, which lies at 0 eV. There is no visible Fermi edge as in the case of metals. The VB maxima (VBM) has been determined by linear extrapolation of the onset of the spectrum to the background. The VBM of the 6H–SiC substrate is estimated to be 2.9 eV below the E_F, and 280.9 eV above the C 1*s* core level, which is consistent with earlier results [51, 52]. The p-GaN VBM amounts to 2.7 eV below the E_F, and 17.7 eV above the Ga 3*d* core line, which is in line with other works [49]. The VBM position shows a shortage of the p-type charges — this behaviour was also observed by Long and McIntyre [53].

The MgO bandgap widths are set down from inelastic energy losses of the O 1*s* and Mg 2*p* core levels for MgO on 6H–SiC [54] and GaN [25] films, respectively (see Fig. 3a and c). For 5 nm thick films, bandgap widths are equal to 6.9 ± 0.2 eV on GaN and 6.7 ± 0.2 eV on SiC. The bandgap for the 3 nm film on SiC is slightly narrower and it amounts to 6.5 ± 0.2 eV. For 2 nm film on GaN it is impossible to determine the bandgap width with reasonable accuracy. When the bulk MgO bandgap is assumed to be equal to 7.8 eV, the surface bandgap appears to be narrower than in the bulk [26] and might be even as narrow as 1 eV for very thin films, nonetheless, usually it does not exceed a range of 5–7 eV [55].

The electron affinity (EA) has been calculated from the equation EA $= h\nu - W - E_g$. Here, $h\nu = 21.2$ eV is the photon energy of the source, W is the difference between the VBM and the cut-off energy of photoemission of the spectrum (E_{cutoff}), and E_g is the bandgap width of the material ($E_g^{\mathrm{SiC}} = 3.0$ eV, $E_g^{\mathrm{GaN}} = 3.4$ eV). The EA of the bare 6H–SiC and p-GaN substrates amounts to 4.0 eV and 3.4 eV, respectively. The work functions (WFs) of the substrates are determined to be 4.1 eV for both and were calculated using the formula WF $= h\nu - E_{\mathrm{cutoff}}$. These values are consistent with other studies [56, 57]. Knowing the bandgap of MgO layers of the investigated systems and the width of the UPS spectra ($W_{\mathrm{MgO/GaN}} = 13.5$ eV, $W_{\mathrm{MgO/SiC}} = 13.7$ eV), the EA of both systems is calculated to be 0.8 eV, which is in line with the results of previous studies [58].

The valence band offset (VBO) and the conduction band offset (CBO) in terms of the binding energy difference ΔE_{CL} between the core levels (CL) of the semiconducting substrate from one side of the interface and the oxide film as an insulator from the other side might be evaluated from two equations

$$\mathrm{VBO} = \Delta E_{\mathrm{CL}} + (E^s_{\mathrm{CL}} - E^s_{\mathrm{VBM}}) - (E^d_{\mathrm{CL}} - E^d_{\mathrm{VBM}}), \quad (1)$$

and

$$\mathrm{CBO} = E^d_{\mathrm{g}} + \mathrm{VBO} - E^s_{\mathrm{g}}. \quad (2)$$

Terms $(E^s_{\mathrm{CL}} - E^s_{\mathrm{VBM}})$ and $(E^d_{\mathrm{CL}} - E^d_{\mathrm{VBM}})$ are the valence band maxima with reference to core level positions for semiconductor and the insulator relevantly. Symbols E^d_g and E^s_g are the corresponding bandgap widths. Since C 1s core level of bare SiC substrate is positioned at $E^{\mathrm{SiC}}_{\mathrm{C}\,1s} = 283.6$ eV (see Fig. 1a) and Mg 2p core level from a 5 nm-MgO/SiC film at $E^{\mathrm{MgO}}_{\mathrm{Mg}\,2p} = 50.9$ eV (see Fig. 1c), the value of ΔE_{CL} for this system is 232.7 eV. Considering $E^{\mathrm{SiC}}_{\mathrm{VBM}} = 2.9$ eV as well as $E^{\mathrm{MgO}}_{\mathrm{VBM}} = 4.4$ eV (see Fig. 3b), the $(E^{\mathrm{SiC}}_{\mathrm{C1s}} - E^{\mathrm{SiC}}_{\mathrm{VBM}})$ term amounts to 281.0 eV and the $(E^{\mathrm{MgO}}_{\mathrm{Mg}\,2p} - E^{\mathrm{MgO}}_{\mathrm{VBM}})$ term to 46.5 eV. Substituting the above data into (1) results in the VBO value equal to 1.8 eV. Putting the last value into (2) under the assumption that $E^s_g \equiv E^{\mathrm{SiC}}_g$ and $E^d_g \equiv E^{\mathrm{MgO}}_g$, the CBO value of 1.9 eV is obtained.

The energy band diagram of the MgO/p-6H–SiC(0001) heterojunction for a 5 nm thick MgO thin film is shown in Fig. 4a. Using the same algorithm as above results in the values VBO = 1.2 eV and CBO = 2.3 eV for the MgO/p-GaN(0001) heterojunction of the same 5 nm MgO film. The energy diagram of this junction is shown in Fig. 4b.

The band bending of the bare substrates, induced by the pinning of the Fermi level at the surface states is visible in both cases. Assuming the bulk Fermi level of both materials is positioned 0.2 eV above the top of the valence band, the band banding of the bare substrates is equal to 2.7 eV and 2.5 eV for the SiC(0001) and GaN(0001) surfaces, respectively. It should be noted that these

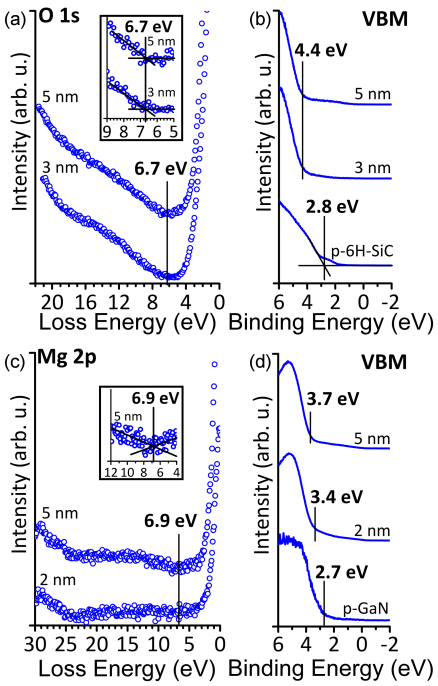

Fig. 3. (a) The bandgap widths of the MgO films as determined from the onset of O 1s energy loss spectra. (b) Positions of valence band maxima on the UPS valence band spectra taken for the bare p-6H–SiC substrate and for a 3 and 5 nm thick MgO films deposited on it. (c) The Mg 2p energy loss spectra measured for the MgO/p-GaN films 2 and 5 nm thick; the bandgap width is possible to be determined for a 5 nm thick MgO film. (d) Positions of valence band maxima on the UPS spectra of the MgO/p-GaN system.

bending may be slightly flattened due to surface photovoltage (SPV) caused by photon illumination from X-ray or UV sources [59]. Even though the substrates are p-type, the surface Fermi levels are closer to the conduction band minimum than to the valence band maximum.

After creating interfaces, the bands of the substrates are getting flattened (relative to the bare surfaces) by 0.3 eV and 0.2 eV for MgO/SiC and MgO/GaN, respectively. There are two factors responsible for the observed flattening. The first one results from the fact that electrons fill out the phase boundary states connected with near-surface defects introduced during the oxide-semiconductor junction formation. Since the MgO layers do not grow epitaxially, thus the growth favors the formation of defects. The second factor results from the above mentioned SPV-assisted effect [57]. The flattening values obtained here are estimated indirectly and cannot be determined directly from the UPS spectra due to the overlap of the electron states of the substrate with the electron states of the MgO layer. They are estimated based on the C 1s and Ga 3d core level lines displacements after

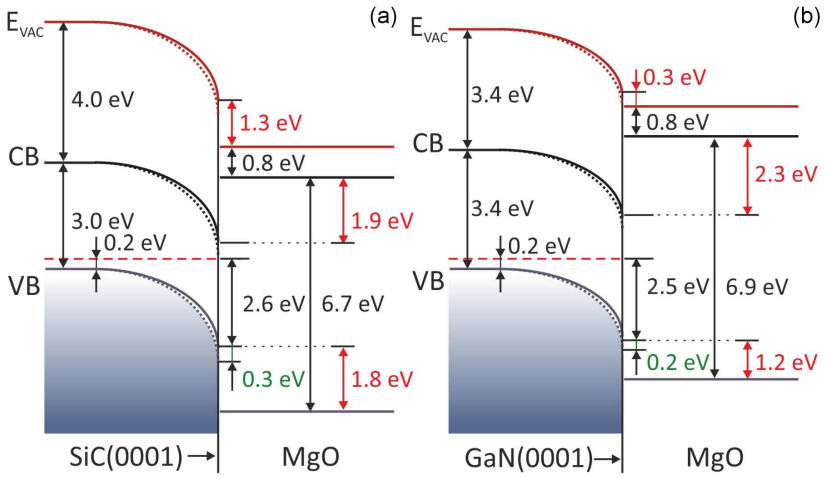

Fig. 4. Band alignment of junctions formed by 5 nm thick MgO thin films deposited on (a) p-6H–SiC(0001) and (b) p-GaN(0001) substrates. Band bending of the bare substrates is marked by dotted line. Flattening of semiconductor bands caused by semiconductor–insulator interface formation is visible. Red values correspond to the band and vacuum level offsets at the interfaces. Green values refer to the reduction in band bending magnitudes. See text for details.

the MgO film deposition and the fact that the energy distances between these peaks and the valence band maximum are constant. The mean free path for electrons from the core level lines is longer than for electrons from the valence band — that is why the peaks from the substrates are visible. The difference in the VBM position for the bare substrate and after MgO deposition leads to lowering of the vacuum level by 1.3 eV for MgO/p-6H–SiC and 0.3 eV for MgO/p-GaN. For both systems, the electron affinity value is 0.8 eV. The band offset values determined here for the MgO/p-6H–SiC(0001) and MgO/p-GaN(0001) heterojunctions meet the requirements for the band discontinuity values demanded for device operating at high temperatures [13, 27].

4. Conclusions

It has been shown that MgO thin layers can be deposited by electron beam evaporation. Combined XPS and UPS methods were employed to characterize the physical and chemical properties of MgO/6H–SiC and MgO/GaN heterojunctions at RT. LEED measurements carried out after the cleaning procedure revealed the diffraction pattern of ordered (1×1) structure observed for the 6H–SiC and p-GaN substrates. No diffraction patterns were observed for MgO layers. The MgO/6H–SiC heterojunction VBO and CBO are calculated to be 1.8 eV and 1.9 eV, respectively. In the case of the MgO/GaN heterojunction, the VBO and CBO are equal to 1.2 eV and 2.3 eV, respectively. The studied heterojunction may act as a barrier for carriers due to sufficient band offsets values.

Acknowledgments

The authors would like to thank K. Świstak for correcting the manuscript.

References

[1] M. Coll, J. Fontcuberta, M. Althammer et al., *Appl. Surf. Sci.* **482**, 1 (2019).

[2] J.A. Cooper, D.T. Morisette, *IEEE Electron. Dev. Lett.* **41**, 892 (2020).

[3] R.S. Pengelly, S.M. Wood, J.W. Milligan, S.T. Sheppard, W.L. Pribble, *IEEE Trans. Microw. Theory Tech.* **60**, 1764 (2012).

[4] M. Ostling, R. Ghandi, C.M. Zetterling, in: *Proc. Int. Symp. Power Semicond. Devices ICs*, 2011, p. 10.

[5] M. Cabello, V. Soler, G. Rius, J. Montserrat, J. Rebollo, P. Godignon, *Mater. Sci. Semicond. Process.* **78**, 22 (2018).

[6] C.T. Ma, Z.H. Gu, *Electronics* **8**, 1401 (2019).

[7] I. Akasaki, H. Amano, *Jpn. J. Appl. Phys.* **36**, 5393 (1997).

[8] F. Roccaforte, P. Fiorenza, G. Greco, M. Vivona, R. Lo Nigro, F. Giannazzo, A. Patti, M. Saggio, *Appl. Surf. Sci.* **301**, 9 (2014).

[9] F. Roccaforte, A. Frazzetto, G. Greco et al., *Appl. Surf. Sci.* **258**, 8324 (2012).

[10] T. Narita, H. Yoshida, K. Tomita et al., *J. Appl. Phys.* **128**, 090901 (2020).

[11] B. Luo, J.W. Johnson, J. Kim et al., *Appl. Phys. Lett.* **80**, 1661 (2002).

[12] B. Luo, J.W. Johnson, B.P. Gila et al., *Solid State Electron.* **46**, 467 (2002).

[13] J. Robertson, B. Falabretti, *J. Appl. Phys.* **100**, 014111 (2006).

[14] J. Robertson, *J. Vac. Sci. Technol. B* **18**, 1785 (2000).

[15] M.D. Losego, H.S. Craft, E.A. Paisley, S. Mita, R. Collazo, Z. Sitar, J.P. Maria, *J. Mater. Res.* **25**, 670 (2010).

[16] T.L. Goodrich, Z. Cai, K.S. Ziemer, *Appl. Surf. Sci.* **254**, 3191 (2008).

[17] B.P. Gila, J. Kim, B. Luo, A. Onstine, W. Johnson, F. Ren, C.R. Abernathy, S.J. Pearton, *Solid State Electron.* **47**, 2139 (2003).

[18] H.S. Craft, J.F. Ihlefeld, M.D. Losego, R. Collazo, Z. Sitar, J.P. Maria, *Appl. Phys. Lett.* **88**, 98 (2006).

[19] D.J. Pingstone, Ph.D. Thesis, University of York, 2018.

[20] O.N. Ogidi-Ekoko, J.C. Goodrich, A.J. Howzen, M.R. Peart, N.C. Strandwitz, J.J. Wierer, N. Tansu, *Solid State Electron.* **172**, 107881 (2020).

[21] C. Bondoux, P. Prené, P. Belleville, F. Guillet, S. Lambert, B. Minot, R. Jérisian, *J. Eur. Ceram. Soc.* **25**, 2795 (2005).

[22] R. Lewandków, P. Mazur, A. Trembułowicz, A. Sabik, R. Wasielewski, M. Grodzicki, *Materials (Basel)* **14**, 1 (2021).

[23] J.J. Chen, B.P. Gila, M. Hlad, A. Gerger, F. Ren, C.R. Abernathy, S.J. Pearton, *Appl. Phys. Lett.* **88**, 1 (2006).

[24] J. Kang, S. Tongay, J. Zhou, J. Li, J. Wu, *Appl. Phys. Lett.* **102**, 012111 (2013).

[25] T. Wook Heo, S. Hwan Moon, S. Young Park, J. Hyuk Kim, H. Joon Kim, *J. Electrochem. Soc.* **154**, J352 (2007).

[26] S. Heo, E. Cho, H.I. Lee, G.S. Park, H.J. Kang, T. Nagatomi, P. Choi, B.D. Choi, *AIP Adv.* **5**, 077167 (2015).

[27] B.L. Zhang, F.F. Cai, G.S. Sun et al., *Appl. Phys. Lett.* **93**, 1409 (2008).

[28] J.M. Hill, D.G. Royce, C.S. Fadley, L.F. Wagner, F.J. Grunthaner, *Chem. Phys. Lett.* **44**, 225 (1976).

[29] M.F. Ebel, H. Ebel, K. Hirokawa, *Spectrochim. Acta B* **37**, 461 (1982).

[30] M.P. Seah, S.J. Spencer, *Surf. Interface Anal.* **33**, 640 (2002).

[31] H. Iwai, J.S. Hammond, S. Tanuma, *J. Surf. Anal.* **15**, 264 (2009).

[32] G. Greczynski, L. Hultman, *Prog. Mater. Sci.* **107**, 100591 (2020).

[33] G. Greczynski, L. Hultman, *Appl. Surf. Sci.* **451**, 99 (2018).

[34] G. Greczynski, L. Hultman, *ChemPhysChem* **18**, 1507 (2017).

[35] T. Seyller, K.V. Emtsev, F. Speck, K.Y. Gao, L. Ley, *Mater. Sci. Forum* **556–557**, 701 (2007).

[36] M. Grodzicki, P. Mazur, R. Wasielewski, A. Ciszewski, *Vacuum* **146**, 216 (2017).

[37] P. Mazur, L. Markowski, *Surf. Interface Anal.* **42**, 1561 (2010).

[38] R. Lewandków, M. Grodzicki, P. Mazur, A. Ciszewski, *Vacuum* **177**, 2 (2020).

[39] K. Idczak, P. Mazur, S. Zuber, L. Markowski, *Appl. Phys. A Mater. Sci. Process.* **122**, 268 (2016).

[40] P. Ciochoń, M. Marzec, N. Olszowska, J. Kołodziej, *Appl. Surf. Sci.* **528**, 146917 (2020).

[41] I. Kusunoki, Y. Igari, *Appl. Surf. Sci.* **59**, 95 (1992).

[42] M. Grodzicki, P. Mazur, R. Wasielewski, A. Ciszewski, *Opt. Appl.* **43**, 91 (2013).

[43] M. Grodzicki, R. Wasielewski, S.A. Surma, A. Ciszewski, *Acta Phys. Pol. A* **116**, 82 (2009).

[44] D. Ferrah, J. Penuelas, C. Bottela, G. Grenet, A. Ouerghi, *Surf. Sci.* **615**, 47 (2013).

[45] B.V. Crist, *Handbooks of Monochromatic XPS Spectra: The Elements and Native Oxides*, Wiley, USA 2000.

[46] B. Wu, Y. Zhao, H. Nan et al., *Nano Lett.* **16**, 3754 (2016).

[47] J.S. Corneille, J. He, D.W. Goodman, *Surf. Sci.* **306**, (1994).

[48] A.V. Naumkin, A. Kraut-Vass, S.W. Gaarenstroom, C.J. Powell, *NIST X-ray Photoelectron Spectroscopy Database*, 2012.

[49] D. Majchrzak, M. Grodzicki, P. Ciechanowicz, J.G. Rousset, E. Piskorska-Hommel, D. Hommel, *Acta Phys. Pol. A* **136**, 585 (2019).

[50] R. Lewandków, M. Grodzicki, P. Mazur, A. Ciszewski, *Surf. Interface Anal.* **53**, 118 (2021).

[51] J.R. Waldrop, R.W. Grant, *Appl. Phys. Lett.* **68**, 2879 (1995).

[52] J.R. Waldrop, *J. Appl. Phys.* **75**, 4548 (1994).

[53] R.D. Long, P.C. McIntyre, *Materials (Basel)* **5**, 1297 (2012).

[54] K.Y. Gao, T. Seyller, L. Ley, F. Ciobanu, G. Pensl, A. Tadich, J.D. Riley, R.G.C. Leckey, *Appl. Phys. Lett.* **83**, 1830 (2003).

[55] P.G. Mather, J.C. Read, R.A. Buhrman, *Phys. Rev. B* **73**, 205412 (2006).

[56] R. Lewandków, M. Grodzicki, P. Mazur, A. Ciszewski, *Vacuum* **177**, 109345 (2020).

[57] M. Grodzicki, P. Mazur, A. Sabik, *Appl. Surf. Sci.* **512**, 145643 (2020).

[58] J.W. Lee, *New Phys. Sae Mulli.* **67**, 1168 (2017).

[59] M. Grodzicki, K. Moszak, D. Hommel, G.R. Bell, *Appl. Surf. Sci.* **533**, 147416 (2020).